文章编号：1001-9014(2024)02-0226-09

DOI:10.11972/j.issn.1001-9014.2024.02.012

Difference and parameter analysis of LST inversion based on Landsat data

WAN Ji-Kang[1*], SHEN Zhe-Hui[2], LI Shan[3]

(1. School of Computer Science and Communication Engineering, Jiangsu University, Zhenjiang 212013, China;
2. College of Civil Engineering, Nanjing Forestry University, Nanjing 210037, China;
3. School of Economics and Management, Fuzhou University, Fuzhou 350108, China)

Abstract: The correct use of the product is possible only when the land surface temperature (LST) data is calculated by an accurate and reliable inversion algorithm. In this paper, we compare the inversion results of five commonly used LST inversion algorithms based on Landsat-8, Landsat-9 data, and weather station data. The inversion results and parameter sensitivity analysis of different algorithms are tested. The results show that the inversion results of the Radiative Transfer Equation (RTE) and Single Channel (SC) algorithms calculated based on land surface emissivity (LSE) are in good agreement with the ground measured. The inversion results of the SC algorithm based on the atmospheric water vapor inversion and the Split Window (SW) algorithm based on the atmospheric water vapor inversion are higher than the measured temperature. The inversion accuracy of the Mono Window (MW) algorithm based on average temperature parameters is not ideal. In addition, the consistency of the inversion temperature of the two data on different ground objects is compared. Our study can provide a reference for land surface temperature inversion based on Landsat-9 data.

Key words: Landsat data, LST, inversion algorithm, accuracy evaluation, stability test, parameter analysis

基于Landsat数据的地表温度反演差异及参数分析

万继康[1*], 沈哲辉[2], 李 珊[3]

(1. 江苏大学 计算机科学与通信工程学院,江苏 镇江 212013;
2. 南京林业大学 土木学院,江苏 南京 210037;
3. 福州大学 经济与管理学院,福建 福州 350108)

摘要:只有基于准确的地表温度反演算法计算出的产品数据,才能正确推广使用。研究基于Landsat-8、Landsat-9和气象站数据,对比了5种常用地表温度反演算法的结果,并对不同算法的反演结果和参数灵敏度进行了测试。结果表明:基于地表比辐射率参数计算的辐射传输方程和单通道算法反演结果与地面实测数据吻合较好。基于大气水汽参数计算的单窗算法和劈窗算法的反演结果均高于实测温度。基于平均温度参数计算的单窗算法反演精度误差较大。此外,比较了两种遥感数据在不同地物上反演温度的一致性。研究结果可为地表温度反演和产品选择提供参考。

关 键 词:Landsat数据;地表温度;反演算法;精度评价;稳定性试验;参数分析

中图分类号:TP79 **文献标识码**:A

Introduction

Land surface temperature (LST) is an important variable in climate and environmental research, which has been widely used in global climate change[1-2], drought monitoring and warning[3], urban heat island[4-6], urban livable assessment[7], satellite precipitation[8], hydrological and ecological effects[9], crop growth monitoring and assessment[10]. The development of high precision temperature data sets with the appropriate resolution is of great significance to any kind of ecological environment research worldwide.

Many researchers have developed algorithms based

Received date: 2023-06-28, **revised date**: 2023-08-21 **收稿日期**:2023-06-28,**修回日期**:2023-08-21

Foundation items: Supported by the National Natural Science Foundation of China (42301385)

Biography: Wan Jikang(1992-), male, Heze, lecturer. Research interests include remote sensing image processing. E-mail: jackvanvip@163.com

[*] **Corresponding author**: Email: jackvanvip@163.com

on surface temperature inversion. Major LST inversion algorithms include RTE[11-12], which is a direct method for LST retrieval using a single TIRS band, the parameters required for inversion mainly include the atmospheric transmittance, surface reflectivity, atmospheric upwelling radiation and atmospheric downwelling radiation. The process calculation of RTE is complicated, but the accuracy of the obtained result is relatively high. The SC algorithm[13-15] includes two calculation methods. The first one is based on the calculation of atmospheric water vapor parameters, the calculation process is simple, but the calculation accuracy is poor. The second method is based on the calculation of atmospheric transmittance, atmospheric upward radiation, atmospheric downward radiation and other parameters. The calculation process of this method is relatively simple and the calculation result has a relatively high precision, so it is also a common method for USGS to produce surface temperature data. The MW algorithm[16] is an algorithm developed specifically for Landsat data, which needs to use parameters including surface emissivity, atmospheric transmittance, and average atmospheric temperature. Due to the huge variation of the estimated mean atmospheric temperature, the inversion accuracy of the MW algorithm is relatively poor. The SW algorithm[13, 17-19] uses two thermal infrared bands for calculation. Because the eleventh band calibration of Landsat is not stable, the inversion accuracy of this algorithm is the worst compared with the above.

In these LST inversion algorithms, multiple basic parameters need to be input[20]. Multiple parameters are estimated variables, not standard variables. Each algorithm is tested on the satellite data for which it is applicable, and sometimes not always applicable faced with new satellite data. For example, the split window algorithm is not suitable for Landsat 8 data, because the calibration of the 11th band is not accurate. It is therefore necessary to evaluate land surface temperature inversion for each new type of satellite data[21].

1 Research data

The study area was chosen to be covered by both Landsat 8 and Landsat 9 data, shown in Fig. 1. The data track number was 123, 032. It mainly covered Beijing. We selected Landsat 8 data with imaging date of November 26, 2021, and Landsat 9 data with imaging date of November 22, 2021 (test data), which were the two images closest to the USGS release date, four days apart. For four days we don't think anything has changed on the surface. The main variation is the influence of atmospheric aerosols and other parameters on temperature inversion, and the data needs to be normalized in the comparative study.

Accurate measurements from 20 meteorological stations (marked in green in Fig. 1) were selected as the true values. The temperature measuring device at the weather station was located 1.5 meters above the ground and recorded data every hour. It is necessary to convert the measured data from the meteorological station to ground data when using the measured data from the meteorological station.

In the inversion of surface temperature in this study, LSE, atmospheric transmittance, upward radiation, downward radiation, atmospheric water vapor content, atmospheric average temperature, and other parameters required by various inversion algorithms are obtained by USGS using interpolation measurements from various stations around the world. A description of the parameter dataset can be found in the USGS official documentation.

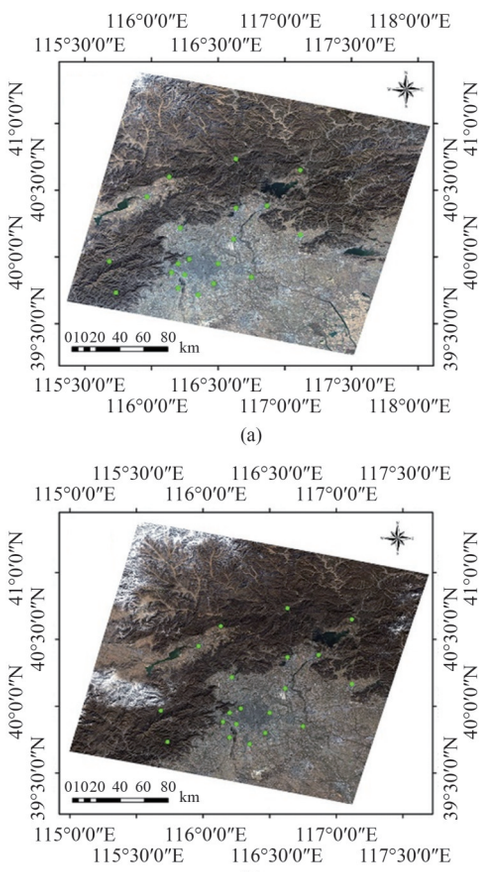

Fig. 1 Study areas, (a) the remote sensing data of 'LC08_L1TP_123032_20211126_20211201_02_T1'; (b) the remote sensing data of 'LC09_L1TP_123032_20211122_20220120_02_T1', with green dots representing the location of the meteorological station

图 1 研究区,(a) Landsat-8 遥感数据:LC08_L1TP_123032_20211126_20211201_02_T1;(b) Landsat-9 遥感数据:LC09_L1TP_123032_20211122_20220120_02_T1,图中绿色荧光点代表气象站点位置

2 Methods

In the data pre-processing stage, the atmospheric correction was mainly carried out on the selected Landsat-8 and Landsat-9 level-1 product data. Then, we combined five commonly used LST inversion algorithms using land surface emissivity, upward radiation, downward radiation, atmospheric water vapor, and average temperature. LST inversion was performed for the corrected atmospheric data. Secondly, we fitted the five temperature in-

version results with the in-situ measurement results of weather stations to compare the accuracy of the five algorithms. The sensitivity of each dependent parameter of the inversion algorithm was tested by controlling the parameters with an equal step size. Finally, we classified the study area, and several pixels were randomly selected for data statistics in each category in the study area and we measured the stability of each inversion algorithm on Landsat-8 and Landsat-9 data according to the mean and standard deviation. The overall process is shown in Fig. 2.

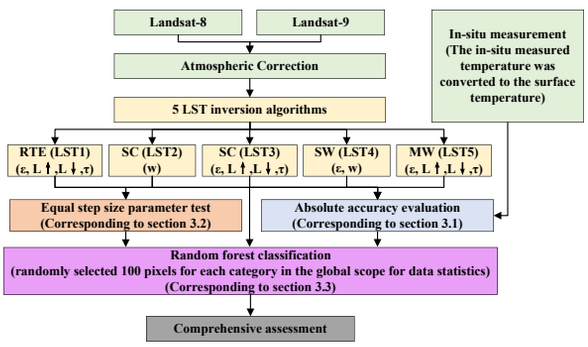

Fig. 2 Overall research process, ε represents land surface emissivity, w represents water vapor content, ($g\cdot cm^{-2}$), $L\downarrow$ represents downwelling radiance, ($W/m^2/sr/um$), $L\uparrow$ represents upwelling radiance, ($W/m^2/sr/um$), τ represents atmospheric transmittance

图2 研究流程图,ε代表地表比辐射率,w代表大气水汽含量,$L\downarrow$代表下行辐量度,$L\uparrow$代表上行辐亮度,τ代表大气透过率

2.1 LST inversion algorithm

Five LST inversion schemes are discussed in this study, which are shown in Table 1.

Table 1 Different LST inversion methods
表1 不同地表温度反演方法

Model	Model + parameter	Model ID
RTE	RTE (LSE, τ, $L\uparrow$, $L\downarrow$)	LST1
SC	SC (w)	LST2
	SC (LSE, τ, $L\uparrow$, $L\downarrow$)	LST3
SW	SW (by Jiménez-Muñoz et al.) (LSE, w)	LST4
MW	MW (LSE, τ, $L\uparrow$, $L\downarrow$, Ta)	LST5

LST1→ Radiative transfer equation (RTE) is a method of surface temperature inversion using a single thermal infrared band. This can be given by Eq. (1):

$$L_\lambda = \left[\varepsilon B(T_s) + (1-\varepsilon)L\downarrow\right]\tau + L\uparrow \quad , \quad (1)$$

where L_λ ($w\cdot m^{-2}\cdot sr^{-1}\cdot \mu m^{-1}$) is the brightness value of the band λ. $B(T_s)$ is the blackbody radiance energy. For more detailed parameter description, please read the original literature[11-12, 22].

LST2→ The Single channel (SC) algorithm can be expressed by Eq. (2) and Eq. (3):

$$T_s = \gamma\left[\varepsilon^{-1}(\psi_1 L + \psi_2) + \psi_3\right] + \delta \quad , \quad (2)$$

$$\gamma = T^2/(b_\gamma L), \delta \approx T - T^2/b_\gamma \quad , \quad (3)$$

where b_γ is equal to 1 320 K for Band 10. ψ_1, ψ_2, ψ_3 are functions of water vapor content (w). For more detailed parameter description, please read the original literature[14].

LST3→ When w in the SC algorithm is greater than 3 $g\cdot cm^{-2}$, Jiménez-Muñoz suggests using Eq. (4) to calculate ψ_1, ψ_2 and ψ_3. This algorithm is the USGS official method for producing LST datasets.

$$\psi_1 = 1/\tau, \psi_2 = -L\downarrow - L\uparrow/\tau, \psi_3 = L\downarrow \quad . \quad (4)$$

LST4→ Some researchers refer to the split window (SW) algorithm of MODIS satellite and transfer it to Landsat data, which can be calculated by Eq. (5):

$$T_s = T_{10} + c_1(T_{10} - T_{11}) + c_2(T_{10} - T_{11})^2 + c_0 + (c_3 + c_4 w)(1 - \varepsilon_m) + (c_5 + c_6 w)\Delta\varepsilon \quad , \quad (5)$$

where T_{10} and T_{11} are the brightness temperatures. $\Delta\varepsilon$ is the LSE difference of Band 10 and Band 11. For more detailed parameter description, please read the original literature[13].

LST5→ The Mono Window (MW) algorithm can be expressed by Eq. (6):

$$T_s = \left\{a\cdot(1-C-D) + \left[b\cdot(1-C-D) + C + D\right]\cdot T - D\cdot T_a\right\}/C, \quad (6)$$

where $a = -67.35$ and $b = 0.45$ of Band 10, T_a is the mean temperature. $C = \varepsilon\cdot\tau$ and $D = (1-\tau)\left[1 + (1-\varepsilon)\cdot\tau\right]$. For more detailed parameter description, please read the original literature[23].

We fitted the five kinds of inversion LST with the temperature measured in situ by the weather station (from near-surface temperature to LST). The T-based technique was used to evaluate the fitting data[23-26]. Root mean square error (RMSE) and average BIAS[27] were used as evaluation criteria in this study. The formulas of these metrics are given by:

$$RMSE = \sqrt{\frac{\sum[T_{Landsat} - T_{station}]^2}{n}} \quad , \quad (7)$$

$$BIAS = \frac{\sum[T_{Landsat} - T_{Station}]^2}{n} \quad , \quad (8)$$

where $T_{Landsat}$ and $T_{Station}$ are the Landsat-8 and Landsat-9 derived LST and in-situ LST, respectively, and n represents the number of in-situ measurements. In this study, in-situ measurement data of 20 meteorological stations were used, so n=20.

2.2 Parameter sensitivity test

Sensitivity analysis of model parameters is an application of a model output error (fuzzy approximation, large number, statistical or other) that is inversely partitioned and inversely assigned to different sources of uncertainty in the model input[28]. We consider the inversion parameters of surface temperature in different places as independent variables and separately control the changes of each parameter to observe the influence of the changes of various parameters on the results. First, assume that with the image after the atmospheric correction by one pixel, the DN value is a fixed value. Then, according to experience, the parameters are selected as control variables, and finally the sensitivity of each pa-

rameter is analyzed. The selected length and step size of each parameter are shown in Table 2.

Table 2　The selection length and step size of each parameter
表 2　选择参数的取值范围和步长

Parameter	Length	Step size
LSE	(0.9, 1.0)	0.01
τ	(0.5, 1.0)	0.01
$L\uparrow$	(0, 5)	0.1
$L\downarrow$	(0, 5)	0.1
w	(0, 2.5)	0.1

To make the results comparable under the same measurement, we normalized the surface temperature. The following equation is utilized:

$$S_e = T_s(x) - T_s(x + \Delta x) \quad , \quad (9)$$

where S_e is the LST difference calculated for each increase in step size; $T_s(x + \Delta x)$ and $T_s(x)$ refer to the LST calculated for "$x + \Delta x$" and "x", respectively.

2.3　Error tests on different ground features

The stability of five inversion algorithms was discussed, and the inversion results on different land use types were selected for statistical analysis. The random forest method was used to classify land use in the study area. Since the accuracy of classification directly affected the test results, the overall classification accuracy was required to be higher than 90%. Considering the spatial resolution of Landsat data and the separability and high precision requirements of land cover, as well as the subsequent research on the thermal environment using surface temperature, we divided land use in the study area into seven categories: water, vegetation, dark buildings, bright soil, dark soil, and high reflectivity buildings. Spectral statistics and analysis were performed for each category, and the specific classification sample selection and classification process, please refer to our previous literature[29].

3　Results and analysis

3.1　Inversion results of different algorithms

Five temperature retrieval algorithms were used to retrieve LST from the Landsat-8 and Landsat-9 data, the results are shown in Fig. 3. It can be seen that the results of each LST inversion algorithm and the graphical trend of the measured data are consistent. This is consistent with our common knowledge that the temperature drops by an average of 6 ℃ for every 1000 meters of elevation. In Fig. 3, the measured data of the high-altitude site is displayed in a concave shape with the adjacent data.

The inversion result values of five temperature inversion algorithms were used to linearly fit the measured temperature values. The fitting results are shown in Fig. 4. It can also be seen from the statistical fitting results that the fitting results of LST1 and LST3 are relatively ideal, and the fitting slope is around 0.7 and R^2 is around 0.6. The best fitting between the model inversion results and the measured results is the mono-window algorithm, which is ideal both in the fitting slope and R^2, and which is the main reason why USGS adopts the MW algorithm. It is worth noting that the fitting slope of LST4 is above 0.9, but R^2 is around 0.45. This phenomenon may be caused by the lack of sample point data on the one hand. Two groups of pixel points are close to the measured points, but the inversion results of some pixel points differ greatly from the measured results of the station. This shows that the stability of the model is poor and the estimation result is not ideal. In addition, the LST2 method based on atmospheric water vapor content parameters and the mono-window algorithm for surface temperature inversion has a lower fitting slope and R^2, which further illustrates the instability of the inversion algorithm based on atmospheric water vapor content parameters.

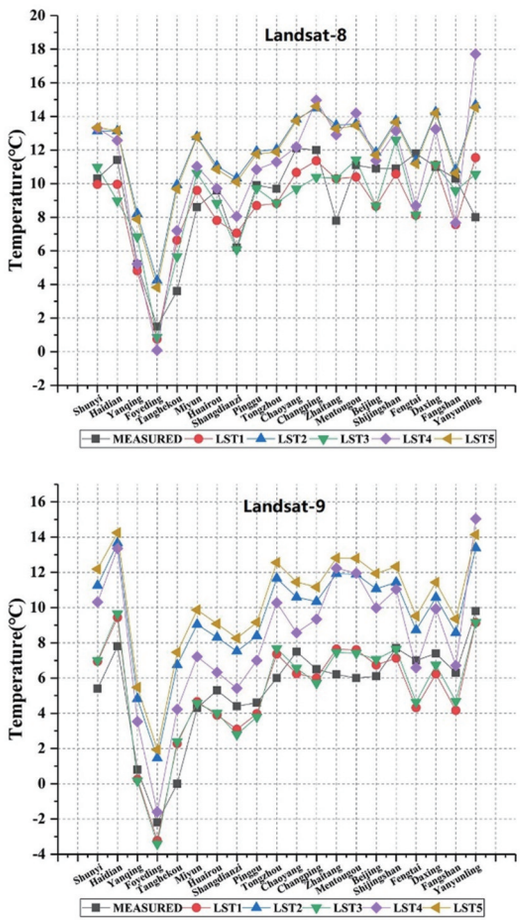

Fig. 3　Inversion results of 5 LST inversion algorithms
图 3　五种地表温度反演算法结果

From the accuracy of the algorithm inversion results and the sensitivity analysis of the parameters in the algorithm, the RTE and SC algorithms calculated using the LSE parameters are better than other algorithms. The MW algorithm yields slightly higher retrieval results than the measured data, and the SW algorithm yields a large difference from the measured data. This may be related

to the unstable radiometric calibration in Band 11 of the Landsat-8 TIRS. In addition, the calibration parameters of the 11th band of Landsat-9 are still being tested. It is hoped that USGS will provide more accurate calibration parameters in the future, and calculate atmospheric influence through two thermal infrared bands to obtain a more accurate surface temperature.

3.2 Sensitivity analysis of model parameters

The inversion temperature of each algorithm was normalized, and the sensitivity of the parameters in the algorithm was analyzed by controlling variables, and the analysis results of each parameter are shown in Fig. 5.

It can be seen from Fig. 5(a) that the atmospheric transmittance variable has a logarithmic function relationship with the inversion result values of the RTE, SC and MW algorithms. As the atmospheric transmittance variable increases, the retrieved surface temperature values gradually decrease. From the curvature shown in the image, the values of the retrieved results of the RTE algorithm change rapidly with the atmospheric transmittance, while the values of the retrieved results of the SC and MW algorithms change slowly with the atmospheric transmittance. In Fig. 5(b), the inversion temperature values of various LST inversion algorithms gradually decrease with the increase of upward radiation parameters. However, the effect of ascending radiation parameters on the LST1 algorithm presents a logarithmic curve, and the effect on the LST3 algorithm presents a linear relationship. In Fig. 5(c), the inversion temperature value of various LST inversion algorithms gradually decreases with the increase of the descending radiation parameter value. However, the influence of down-radiation parameters on LST1 and LST3 shows a linear relationship. The LST inversion results decrease by 0.3 units with each unit increase of downward radiation. As can be seen from Fig. 5(d), the inversion temperature values of various LST inversion algorithms gradually decrease with the increase of ground object-specific emissivity. The effects of specific emissivity parameters on all inversion algorithms show a linear relationship. For every 0.1 units increase

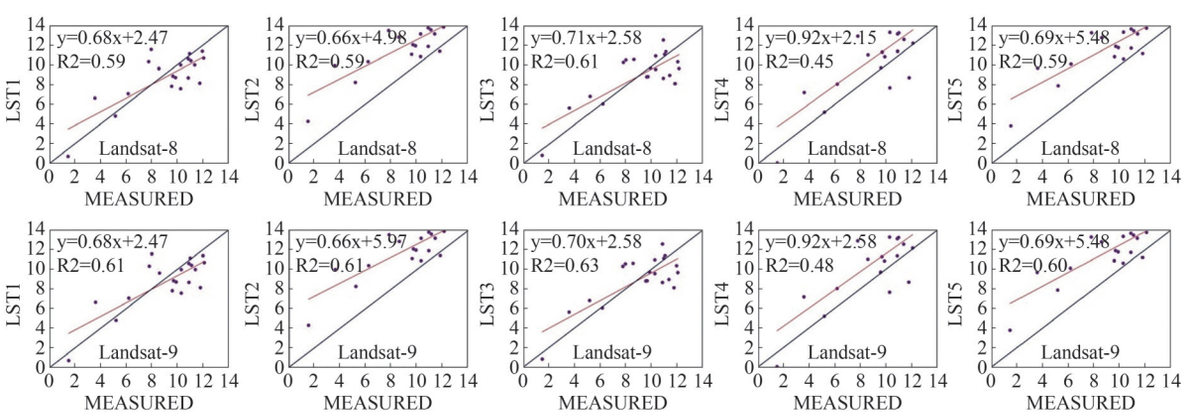

Fig. 4 The inversion results of the algorithm fit the measured values
图4 五种地表温度反演结果与气象站点实测数据拟合

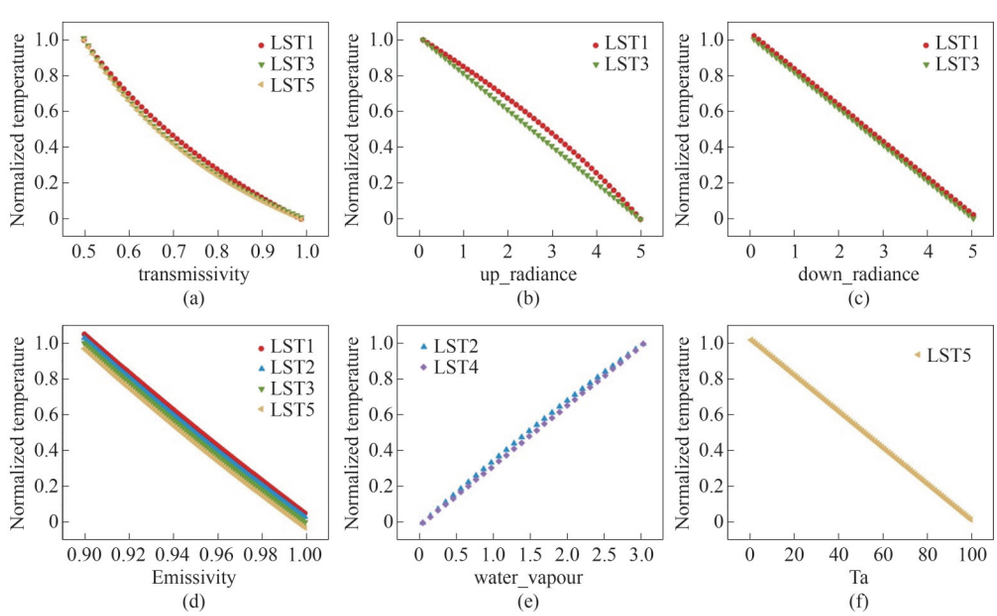

Fig. 5 Parameter sensitivity analysis
图5 参数灵敏度测试

in specific emissivity, the retrieved LST decreases by 1 unit. In Fig. 5(e), the inversion values of LST2 and LST4 gradually increase with the increase of the atmospheric water vapor content. However, the parameters of atmospheric water vapor content show a logarithmic trend to LST2 and a linear relationship to LST4. As can be seen from Fig. 5(f), the inversion value of the LST5 algorithm gradually decreases with the increase of average surface temperature parameters. The influence of average temperature parameters on LST5 shows a linear relationship, and the inversion MW value of average surface temperature decreases by 0.01 units when the average surface temperature increases by 1 unit.

3.3 Stability analysis of different methods

The random forest algorithm was used to classify the land cover in the study area, and then five inversion LSTs were superimposed. The maximum value, minimum value, mean value, and standard deviation of different temperature inversion methods in different types of two images were calculated to indicate the stability of temperature inversion with different temperature inversion methods in different ground covers. We selected 100 pure pixel points in each category and carried out the ground object verification with the data taken by an unmanned aerial vehicle on the imaging day. The statistical results are shown in Table 3-7 and Fig. 6.

As can be seen from Table 3-7 and Fig. 6, the inversion temperature of the five LST inversion algorithms on the water body and vegetation is the most stable, and the percentage error is relatively low among all land cover types. This may be because, on the one hand, the water body and vegetation area are relatively stable, and the temperature change will not be disturbed by too many human factors; on the other hand, the water body and vegetation have relatively high separability. All inversion algorithms for high reflectivity building inversion results are the most unstable, its percentage error is the largest, the possible reason is that high reflectivity buildings are

Table 3　LST1 statistical results
表3　LST1统计结果

Land Cover	Landsat-8 (°C)				Landsat-9 (°C)			
	Max	Min	Mean	Std	Max	Min	Mean	Std
Water	6.234	0.784	2.783	0.576	1.872	−4.324	−2.762	0.425
Vegetation	6.982	4.824	5.234	0.823	2.731	−2.973	0.832	0.756
Dark buildings	24.832	−7.983	5.759	3.320	21.870	−9.832	4.862	3.013
Bright soil	12.0735	−8.089	6.231	4.432	11.872	−6.273	3.281	4.171
Dark soil	10.380	−7.783	0.194	1.471	9.384	−5.923	−0.827	1.362
High reflectivity buildings	22.447	−7.368	4.280	5.39	18.319	−9.873	3.976	4.792

* Please note that the outdoor air temperature was 4 °C on the day the Landsat-8 data was imaged, and −3 °C on the day the Landsat-9 data was imaged. This data can be used as auxiliary reference data to better understand our category statistics.

Table 4　LST2 statistical results
表4　LST2统计结果

Land Cover	Landsat-8 (°C)				Landsat-9 (°C)			
	Max	Min	Mean	Std	Max	Min	Mean	Std
Water	13.345	3.563	7.453	2.544	7.456	−5.649	2.479	2.325
Vegetation	14.682	5.574	8.016	2.690	11.932	−3.973	2.832	2.456
Dark buildings	25.341	−5.398	9.759	4.320	18.840	−8.452	6.862	4.013
Bright soil	23.735	−4.809	8.256	4.472	15.872	−4.743	5.813	4.311
Dark soil	22.120	−6.453	3.944	3.716	18.854	−4.931	1.673	3.326
High reflectivity buildings	26.423	−4.318	7.208	5.321	21.394	−11.354	1.976	4.942

Table 5　LST3 statistical results
表5　LST3统计结果

Land Cover	Landsat-8 (°C)				Landsat-9 (°C)			
	Max	Min	Mean	Std	Max	Min	Mean	Std
Water	5.933	0.882	2.881	0.474	1.832	−4.324	−2.453	0.318
Vegetation	6.745	4.456	5.675	0.857	2.456	−2.675	0.848	0.796
Dark buildings	23.124	−7.875	5.234	3.352	21.345	−9.373	4.367	3.274
Bright soil	21.923	−8.355	6.333	4.245	19.123	−6.171	3.161	4.081
Dark soil	21.485	−7.245	1.245	1.571	17.345	−5.235	−0.145	1.461
High reflectivity buildings	23.232	−7.567	5.846	5.478	22.487	−10.484	3.353	4.863

Table 6 LST4 statistical results
表6 LST4统计结果

Land Cover	Landsat-8 (°C)				Landsat-9 (°C)			
	Max	Min	Mean	Std	Max	Min	Mean	Std
Water	14.234	3.123	6.653	0.977	7.852	−5.321	−1.122	0.855
Vegetation	15.948	7.824	9.234	0.999	8.731	−1.973	2.832	0.966
Dark buildings	28.852	−6.763	6.239	4.328	20.874	−8.835	6.862	4.513
Bright soil	27.075	−8.219	8.222	4.932	15.842	−9.213	5.281	4.672
Dark soil	27.122	−6.213	5.234	3.346	18.314	−8.123	−4.237	3.862
High reflectivity buildings	27.227	−8.234	8.123	5.721	20.391	−13.343	2.342	5.212

Table 7 LST5 statistical results
表7 LST5统计结果

Land Cover	Landsat-8 (°C)				Landsat-9 (°C)			
	Max	Min	Mean	Std	Max	Min	Mean	Std
Water	14.474	3.284	25.734	1.526	3.872	−6.343	−3.722	1.352
Vegetation	13.922	7.821	8.934	1.982	6.721	−5.923	3.823	1.846
Dark buildings	27.456	−9.345	8.234	3.887	20.238	−8.794	2.564	3.713
Bright soil	26.035	−7.349	5.357	4.631	20.412	−7.456	7.567	4.671
Dark soil	27.546	−8.345	4.634	3.575	16.435	−6.456	−3.624	3.387
High reflectivity buildings	28.673	−5.345	6.234	5.593	20.334	−9.834	4.974	4.891

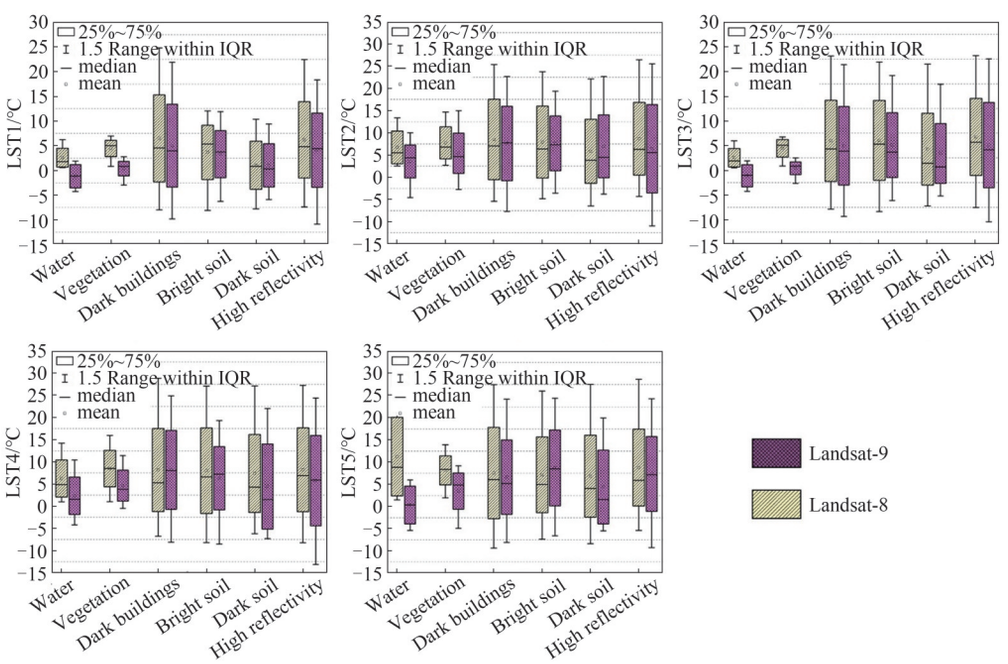

Fig. 6 Stability statistics of five inversion algorithms on different land covers
图6 五种反演算法在不同土地覆盖条件下的稳定性统计

generally factories or large warehouses, its production operation will generate large heat, stop operation will rapidly lose heat, resulting in large fluctuations in statistical data.

4 Discussion

All LST inversion algorithms for Landsat data have certain errors. Such errors can only be minimized, not eliminated. Since the required parameters in the LST inversion algorithm are not exact values, and some parameters need to be estimated initialized, it is very necessary to explore the disturbance of each parameter on the results. All the algorithms that worked for Landsat-8 also worked for Landsat-9 data. However, unlike Landsat-8 data, the radiometric calibration file of Band 11 of Landsat-9 has not been updated yet. We expect USGS to provide more accurate calibration parameters so that we can use the data of the two channels to constrain each other to

obtain higher precision temperature inversion results.

Considering the accuracy and parameter sensitivity of the inversion algorithm, the RTE and SC algorithms using LSE parameters have high accuracy and good algorithm stability. The inversion results of the SC algorithm and SW algorithm based on the calculation of atmospheric water vapor content parameters fit poorly with the measured data. The MW algorithm based on LSE and average atmospheric temperature parameters fit poorly with the measured results. Therefore, we believe that the results obtained by the LSE parameter inversion algorithm are better than those obtained by the atmospheric water vapor content parameter inversion algorithm. By comparing LST1 and LST5, it can be seen that the LST5 algorithm has one more atmospheric average temperature estimation parameter than the LST1 algorithm, leading to a poor fitting effect on inversion results, which may be due to the negative impact of excessive uncertain parameters on results. We strongly recommend LST1 and LST3 algorithms for the LST inversion from Landsat data. Even though it is not possible to find atmospheric profiles (radiosonde data, etc.) in place at any time and in any place, this use (using ACPC to simulate atmospheric profile information) can affect the accuracy of the method, but from our results and the literature[5,12,14-16,18,30-32], NASA's ACPC provided an inversion algorithm with high accuracy. Wang[33] found that SW had the lowest sensitivity to input parameter errors, but the inversion accuracy was not as high as other algorithms. The relationship between the dependence of the inversion algorithm on the parameters and the accuracy of the result needs to be further explored. In a humid environment, parameter error has little effect on the results. Xu[34] compared the inversion results of SC and SW algorithms and concluded that the inversion results of the SC algorithm were significantly better than those of SW, especially when the atmospheric water vapor content was more than 2.5 $g \cdot cm^{-2}$.

In the comparative analysis of all LST inversion model results, error tracing is very necessary. Through error tracing, we can reverse calculate which parameters the error mainly comes from and which parameters have high sensitivity in model calculation. In the subsequent calculation process, various considerations can be taken to reduce the error accumulation. According to the inversion results of different temperature inversion algorithms on different data and different land cover types, we can see that the inversion percentage error of the same inversion algorithm and the same land cover type on Landsat-9 is smaller than that on Landsat-8, indicating that the data quality of Landsat-9 has been improved.

5 Conclusions

The algorithm for Landsat-8 can also be applied to Landsat-9 data. The calculation process of the SC (LST3) algorithm is a little simpler than that of RTE (LST1), but there is little difference in accuracy between the two algorithms. The RTE algorithm and SC algorithm based on LSE parameters are superior to other algorithms in terms of both accuracy of results and sensitivity to parameters. The retrieval results of the SC (LST2) algorithm and SW (LST4) algorithm based on the atmospheric water vapor retrieval are higher than the measured temperature. The inversion effect of the MW (LST5) algorithm based on average temperature parameters is not particularly ideal. This phenomenon shows that among all the current surface temperature inversion algorithms, the accuracy of surface temperature inversion based on the single window algorithm is the highest, which is also the algorithm used in the advanced products released by USGS. However, the starting point of the split window algorithm is to eliminate the error caused by atmospheric influence with the help of two thermal infrared channels, so as to obtain higher inversion accuracy. But the actual result is the opposite. This may be due to unstable radiometric calibration of Landsat-8 TIRS Band 11. Calibration parameters for Band 11 of Landsat-9 are still being tested. It is hoped that USGS will provide more accurate calibration parameters in the future and calculate atmospheric effects through two thermal infrared bands to obtain more accurate surface temperatures.

With the same inversion algorithm and the same ground cover type, the inversion percentage error on Landsat-9 is smaller than that on Landsat-8, indicating that the data quality of Landsat-9 has been improved. From the inversion results of different inversion algorithms on the same data, the results of water and vegetation have good stability.

References

[1] Robeson S M. Relationships between Mean and Standard Deviation of Air Temperature: Implications for Global Warming[J]. *Climate Research*, 2002, **22**(3): 205-213.

[2] Lofgren B M, Hunter T S, Wilbarger J. Effects of Using Air Temperature as a Proxy for Potential Evapotranspiration in Climate Change Scenarios of Great Lakes Basin Hydrology[J]. *Journal of Great Lakes Research*, 2011, **37**(4): 744-752.

[3] Wan Z, Wang P, Li X. Using MODIS Land Surface Temperature and Normalized Difference Vegetation Index products for monitoring drought in the southern Great Plains, USA[J]. *International Journal of Remote Sensing*, 2010, **25**(1): 61-72.

[4] Keeratikasikorn C, Bonafoni S. Urban Heat Island Analysis over the Land Use Zoning Plan of Bangkok by Means of Landsat 8 Imagery [J]. *Remote Sensing*, 2018, **10**(3):440.

[5] Zhou D, Xiao J, Bonafoni S, *et al*. Satellite Remote Sensing of Surface Urban Heat Islands: Progress, Challenges, and Perspectives [J]. *Remote Sensing*, 2018, **11**(1):48.

[6] Sobrino J A, Oltra-Carrió R, Sòria G, *et al*. Evaluation of the surface urban heat island effect in the city of Madrid by thermal remote sensing[J]. *International Journal of Remote Sensing*, 2012, **34**(9-10): 3177-3192.

[7] Tan J, Zheng Y, Tang X, *et al*. The urban heat island and its impact on heat waves and human health in Shanghai[J]. *International Journal of Biometeorology*, 2010, **54**(1): 75-84.

[8] Yong B, Ren L, Hong Y, *et al*. First evaluation of the climatological calibration algorithm in the real-time TMPA precipitation estimates over two basins at high and low latitudes[J]. *Water Resources Research*, 2013, **49**(5): 2461-2472.

[9] Dash P, Göttsche F M, Olesen F S, *et al*. Land surface temperature and emissivity estimation from passive sensor data: Theory and practice-current trends [J]. *International Journal of Remote Sensing*, 2010, **23**(13): 2563-2594.

[10] De Wit A J, van Diepen C A. Crop Growth Modelling and Crop Yield Forecasting Using Satellite-Derived Meteorological Inputs[J]. *International Journal of Applied Earth Observations and Geoinformation*, 2007, **10**(4): 414-425.

[11] Siddiqui A, Kushwaha G, Raoof A, *et al*. Bangalore: Urban heating

or urban cooling?[J]. *The Egyptian Journal of Remote Sensing and Space Science*, 2021, **24**(2): 265-272.
[12] Price J C. Estimating Surface Temperatures from Satellite Thermal Infrared Data——A Simple Formulation for the Atmospheric Effect[J]. *Remote Sensing of Environment*, 1983, **13**: 353-361.
[13] Jiménez-Muñoz J C, Cristobal J, Sobrino J A, *et al*. Revision of the Single-Channel Algorithm for Land Surface Temperature Retrieval From Landsat Thermal-Infrared Data[J]. *IEEE Transactions on Geoscience and Remote Sensing*, 2009, **47**(1): 339-349.
[14] Jiménez-Muñoz J C, Sobrino J A. A Single-Channel Algorithm for Land-Surface Temperature Retrieval From ASTER Data[J]. *IEEE Geoscience and Remote Sensing Letters*, 2010, **7**(1): 176-179.
[15] Jiménez-Muñoz J C, Sobrino J A, Skokovic D, *et al*. Land Surface Temperature Retrieval Methods From Landsat-8 Thermal Infrared Sensor Data[J]. *IEEE Geoscience and Remote Sensing Letters*, 2014, **11**(10): 1840-1843.
[16] Qin Z H, Karnieli A, Berliner P. A mono-window algorithm for retrieving land surface temperature from Landsat TM data and its application to the Israel-Egypt border region[J]. *International Journal of Remote Sensing*, 2010, **22**(18): 3719-3746.
[17] Rozenstein O, Qin Z, Derimian Y, *et al*. Derivation of land surface temperature for Landsat-8 TIRS using a split window algorithm[J]. *Sensors*, 2014, **14**(4): 5768-80.
[18] Mao K, Qin Z, Shi J, *et al*. A practical split-window algorithm for retrieving land-surface temperature from MODIS data[J]. *International Journal of Remote Sensing*, 2007, **26**(15): 3181-3204.
[19] Dozier Z M W a J. A Generalized Split- Window Algorithm for Retrieving Land-Surface Temperature from Space[J]. *IEEE Transactions on geoscience and remote sensing*, 1996, **34**(4): 892-905.
[20] Prasanjit D, Folke S O, Herbert F. Retrieval of Land Surface Temperature and Emissivity from Satellite Data: Physics, Theoretical Limitations and Current Methods[J]. *Journal of the Indian Society of Remote Sensing*, 2001, **29**(1): 24-30.
[21] Yu Y, Tarpley D, Privette J L, *et al*. Validation of GOES-R Satellite Land Surface Temperature Algorithm Using SURFRAD Ground Measurements and Statistical Estimates of Error Properties[J]. *IEEE Transactions on Geoscience and Remote Sensing*, 2012, **50**(3): 704-713.
[22] Wan J K, Zhu M. Accuracy evaluation and parameter analysis of land surface temperature inversion algorithm for Landsat-8 data[J]. *Advance in meteorology*, 2021, (2021).
[23] Zhang Z, He G, Wang M, *et al*. Validation of the generalized single-channel algorithm using Landsat 8 imagery and Surfrad ground measurements[J]. *Remote Sensing Letters*, 2016, **7**(8): 810-816.
[24] Meng X, Cheng J, Zhao S, *et al*. Estimating Land Surface Temperature from Landsat-8 Data using the NOAA JPSS Enterprise Algorithm[J]. *Remote Sensing*, 2019, **11**(2): 155.
[25] Wang M, Zhang Z, Hu T, *et al*. A Practical Single-Channel Algorithm for Land Surface Temperature Retrieval: Application to Landsat series data[J]. *Journal of Geophysical Research: Atmospheres*, 2019, 124(1): 299-316.
[26] Li Z L, Tang B-H, Wu H, *et al*. Satellite-derived land surface temperature: Current status and perspectives[J]. *Remote Sensing of Environment*, 2013, **131**: 14-37.
[27] Sekertekin A, Bonafoni S. Land Surface Temperature Retrieval from Landsat 5, 7, and 8 over Rural Areas: Assessment of Different Retrieval Algorithms and Emissivity Models and Toolbox Implementation[J]. *Remote Sensing*, 2020, **12**(2): 294.
[28] Saltelli A. Sensitivity Analysis for Importance Assessment[J]. *Risk Analysis*, 2002, **22**(3): 579-590.
[29] Wan J K, Zhu M. Contribution degree of different surface factors in urban interior to urban thermal environment[J]. *Advance in meteorology*, 2021(Pt.1): 1843053.
[30] Julia A. Barsi J L B, John R. Schott. An Atmospheric Correction Parameter Calculator for a Single Thermal Band Earth-Sensing Instrument[J]. *IEEE International Geoscience & Remote Sensing Symposium*, 2003: 3014-3016.
[31] Sun J, Salvucci G D, Entekhabi D. Estimates of evapotranspiration from MODIS and AMSR-E land surface temperature and moisture over the Southern Great Plains[J]. *Remote Sensing of Environment*, 2012, **127**: 44-59.
[32] Xu H Q. Evaluation of Two Absolute Radiometric Normalization Algorithms for Pre-processing of Landsat Imagery[J]. *Journal of China University of Geosciences*, 2006, **17**(2): 146-157.
[33] Wang L, Lu Y, Yao Y. Comparison of Three Algorithms for the Retrieval of Land Surface Temperature from Landsat 8 Images[J]. *Sensors*, 2019, **19**(22): 5049.
[34] Xu H Q. Retrieval of reflectivity and surface temperature from the newly launched Landsat 8 satellite[J]. *Chinese journal of geophysice*, 2015, **58**(3): 741-747.